

Magnetic Sensing inside a Diamond Anvil Cell via Nitrogen-Vacancy Center Spins *

Yan-Xing Shang(商延兴)^{1,2†}, Fang Hong(洪芳)^{1†}, Jian-Hong Dai(戴建洪)^{1†}, Hui-Yu(于慧)^{1,2},
Ya-Nan Lu(卢亚男)^{1,2}, En-Ke Liu(刘恩克)^{1,3}, Xiao-Hui Yu(于晓辉)^{1,3**}, Gang-Qin Liu(刘刚钦)^{1**},
Xin-Yu Pan(潘新宇)^{1,3,4**}

¹Beijing National Laboratory for Condensed Matter Physics, Institute of Physics, Chinese Academy of Sciences, Beijing 100190

²School of Physical Sciences, University of Chinese Academy of Sciences, Beijing 100049

³Songshan Lake Materials Laboratory, Dongguan 523808

⁴CAS Center of Excellence in Topological Quantum Computation, Beijing 100190

(Received 9 July 2019)

The diamond anvil cell-based high-pressure technique is a unique tool for creating new states of matter and for understanding the physics underlying some exotic phenomena. *In situ* sensing of spin and charge properties under high pressure is crucially important but remains technically challenging. While the nitrogen-vacancy (NV) center in diamond is a promising quantum sensor under extreme conditions, its spin dynamics and the quantum control of its spin states under high pressure remain elusive. In this study, we demonstrate coherent control, spin relaxation, and spin dephasing measurements for ensemble NV centers up to 32.8 GPa. With this *in situ* quantum sensor, we investigate the pressure-induced magnetic phase transition of a micron-size permanent magnet Nd₂Fe₁₄B sample in a diamond anvil cell, with a spatial resolution of $\sim 2\ \mu\text{m}$, and sensitivity of $\sim 20\ \mu\text{T}/\text{Hz}^{1/2}$. This scheme could be generalized to measure other parameters such as temperature, pressure and their gradients under extreme conditions. This will be beneficial for frontier research of condensed matter physics and geophysics.

PACS: 62.50.-p, 76.70.Hb, 07.35.+k

DOI: 10.1088/0256-307X/36/8/086201

Research into high pressure has opened a new frontier for scientists in various fields, with new materials, structures, and emergent physical properties being reported.^[1] Under high-pressure conditions, simple compounds have shown complicated phase diagrams. For example, eight phases have been reported in dense ice, six in solid oxygen, and six in solid hydrogen,^[2–4] while many pure elements are superconductors under high pressure.^[5] Hydrogen is expected to be a room-temperature superconductor, and many studies have explored its metallic state.^[6] Recently, superconductive behavior in hydride has attracted more attention, as the superconductor phase transition temperature has been reported as being over 260 K,^[7–9] which is the outdoor temperature at most areas in the northern hemisphere winter.

On the other hand, there are scientific and technique challenges associated with high-pressure research. Due to the small sample amounts and delicate high-pressure loading schemes, *in situ* measurements at high pressure of magnetic properties, and of local temperature and pressure, are very difficult.^[10] Taking magnetic sensing as an example, neutron scattering can be used to detect magnetism in a Paris–Edinburgh cell up to 25 GPa. However, the data collecting efficiency is much lower than those in low-pressure

experiments, and a relatively large sample amount is required, which is impossible in ultrahigh pressure experiments.^[1] For diamond anvil cell (DAC)-based experiments, the widely used superconducting quantum interference device (SQUID)^[5] and AC coil magnetometer^[11] have limited magnetic field sensitivity, as the pickup coils are remote from the sample (outside the cell). The lack of *in situ* magnetic field sensing restricts the frontier research of high pressure. For example, one critical feature of the superconducting state, Meissner effect, is still unattainable under ultrahigh pressures.^[8,9] Based on these considerations, an *in situ* and sensitive magnetic sensing scheme for high-pressure studies is in strong demand.

The nitrogen-vacancy (NV) center in diamond has been proposed as a powerful technique to study magnetic and electric phenomena.^[12–15] The NV center spin state is ultrasensitive to local perturbations, such as magnetic and electronic fields, and the working range of this diamond sensor covers a temperature range from mK to 1000 K,^[16] a magnetic field range from zero to 3 T,^[17] and a pressure range from zero to 60 GPa.^[12] At the same time, the techniques for NV spin polarization, control and read out are quite compatible with DAC-based high-pressure techniques. Optically detected magnetic resonance (ODMR) spec-

*Supported by the National Basic Research Program of China under Grant No 2015CB921103, the National Key R&D Program of China under Grant No 2016YFA0401503, the Strategic Priority Research Program of Chinese Academy of Sciences under Grant No XDB28000000, the National Natural Science Foundation of China under Grant Nos 11574386, 11575288 and 51402350, and the Youth Innovation Promotion Association of Chinese Academy of Sciences under Grant No 2016006.

†Yan-Xing Shang, Fang Hong and Jian-Hong Dai contributed equally to this work.

**Corresponding authors. Email: yuxh@iphy.ac.cn; gqliu@iphy.ac.cn; xypan@iphy.ac.cn

© 2019 Chinese Physical Society and IOP Publishing Ltd

tra of diamond NV centers have been measured under high pressures,^[12,18–20] providing static magnetic field information inside DACs.

To fully exploit the quantum nature of diamond NV-based probes, their spin dynamics and the quantum control of the spin states under high pressure are urgently needed. In this work, we demonstrate coherent driving, spin relaxation, and spin dephasing measurements for ensemble NV centers up to 32.8 GPa. With this well-controlled *in situ* quantum sensor, we investigate the pressure-induced magnetic phase transition of a micron-size permanent magnet Nd₂Fe₁₄B sample inside a diamond anvil cell, with a spatial resolution of $\sim 2 \mu\text{m}$, and a sensitivity of $\sim 20 \mu\text{T}/\sqrt{\text{Hz}}$. Our results show that NV-based quantum sensing is a promising technique to study both the static and dynamic magnetic phenomena under high pressures. This scheme can be generalized to measure other physical parameters such as temperature and pressure,^[12,21,22] and will therefore be beneficial for frontier research of condensed matter physics and geophysics.

We start by introducing the working principle of ODMR. This technique is similar to nuclear magnetic resonance and electron paramagnetic resonance, but without the need for a large external magnetic field (polarization) or for pickup coils (readout). NV center is a spin-1 system, with a spin triplet ground state.^[23] As shown in Fig. 1, a green laser pulse of several microseconds is used to polarize NV electron spin to the $m_S = 0$ state with high fidelity, and the following resonant microwave pulse prepares the spin probe to the designed quantum state, e.g., a superposition state of the $m_S = 0$ and $m_S = 1$ states. Then, the interaction between the probe and the sample (and the environment) alters the NV spin states, which could be read out by measuring the NV fluorescence intensity under a second green laser excitation. Note that both the static magnetic field and the dynamic magnetic noise could be detected with this spin sensor (Fig. 1(b)), and a large number of sensing schemes have been developed to meet the challenges of sensing weak signals and to improve the spatial and spectrum resolutions.^[24–28]

To carry out the ODMR measurement under high pressure, a DAC with a low fluorescence background and an assembled microwave antenna have been used, as shown in Fig. 1(a). The high-pressure sample chamber is enclosed by two diamond anvils and a rhenium metal gasket. The microwave transmission line is a piece of thin platinum wire, placed at the center of the sample chamber, which is further connected to the external microwave cable. We use *c*-BN powder mixed with epoxy to insulate the platinum wire from the rhenium gasket. KBr is used as the pressure medium, and a ruby ball ($\sim 5 \mu\text{m}$) is used as the pressure marker.^[29] Diamond particles with ensemble NV centers are randomly dispersed on the DAC culet. The diamond par-

ticles (typically in diameter of $1 \mu\text{m}$ with an NV center density of $\sim 2 \text{ppm}$) are purchased from Adamas Nanotechnologies. A long working distance objective is used to focus the green laser beams onto the DAC culet, and to collect the NV center fluorescence signals there. All experiments are carried out at room temperature.

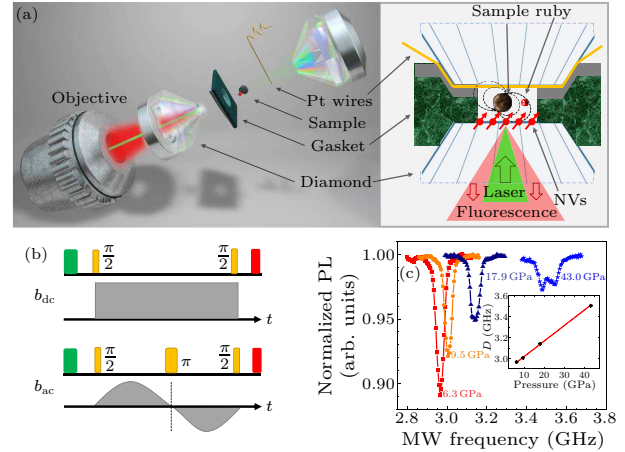


Fig. 1. The principle of quantum sensing under pressures.

Diamond nitrogen-vacancy (NV) centers are quantum sensors sensitive to local perturbations. The magnetic field from the sample alters the spin state of nearby NV centers, which can also be polarized, manipulated and read out remotely, using optical and microwave pulse trains. (a) Experimental setup. A diamond anvil cell (DAC) provides the high-pressure environment. A long working distance objective focuses the excitation laser (532 nm) onto the diamond culet, and collects NV fluorescence there. A platinum wire in diameter of several μm delivers microwave pulses to the sample position, and a nearby ruby particle is used to calibrate pressures. (b) Sensing schemes for dc (top) and ac (bottom) magnetic fields. (c) Optically detected magnetic resonance (ODMR) spectra of NV centers under pressure, with no external magnetic field. Inset: ODMR zero-field splitting D as a function of the applied pressure. The solid line is a linear fitting, with a slope of $dD/dP = 14.9 \pm 0.5 \text{ MHz/GPa}$.

Figure 1(c) shows the zero-field ODMR spectra for ensemble NV centers under different pressures. Under the ambient condition, the ODMR spectrum resonant dip is at 2.87 GHz, which equals the value of the zero-field splitting D of the NV center in diamond. The width of the resonant dip and the Lorentz shape of the spectra are mainly determined by the microwave power broadening effect (weaker microwave driving gives smaller width and less contrast). As the pressure increases, the ODMR spectra shift to the high frequency side. The inset in Fig. 1(c) shows the dependence of the resonant frequency on the applied pressure, a linear function fitting gives a slope of $dD/dP = 14.9 \pm 0.5 \text{ MHz}$, which agrees well with the results reported previously.^[12] As the pressure is greater than 20 GPa, a larger broadening and an extra splitting could be observed. We attribute this extra splitting to the non-hydrostatic pressure, which destroys the C_{3V} symmetry of the NV Hamiltonian and gives the non-degenerated eigen values of the spin = 1

system.^[23] The non-hydrostatic pressure is expected as KBr is a solid pressure medium, and the inhomogeneous pressure distribution in the diamond particle causes the large broadening. These side effects could be suppressed by an external magnetic field, as discussed below.

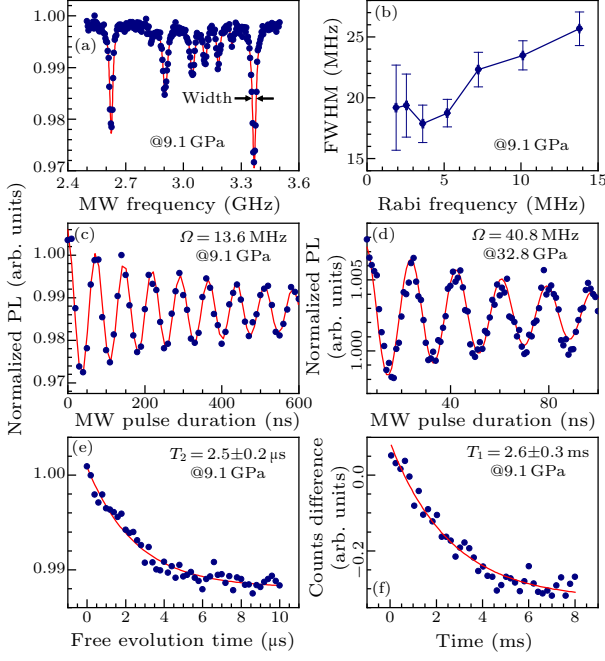


Fig. 2. Coherent quantum control of NV spins under high pressure. (a) Continuous-wave ODMR spectrum of ensemble NV centers in a μm -scale diamond particle. An external magnetic field of ~ 145 Gauss is applied to lift the degeneracy of the four N–V orientations in the diamond crystal. (b) Width of the rightmost ODMR resonant dip as a function of the microwave (MW) power, where the intrinsic width of the resonant dips (~ 20 MHz) is mainly determined by the inhomogeneous broadening of the ensemble NV centers, including local strain and nuclear spin distributions. (c)–(d) Typical Rabi oscillations of NV centers under high pressures, where the red lines are fitting of cosine functions with exponential decay. (e) Typical spin echo and (f) spin relaxation signals of the NV spins under high pressure.

We then characterize the magnetic sensitivity of the NV-based quantum sensors in the DAC. An external magnetic field of ~ 145 Gauss is applied to lift the degeneracy of the four possible N–V orientations in the diamond lattice. The applied pressure is 9.1 GPa. The full ODMR spectrum for a diamond particle on the DAC culet is shown in Fig. 2(a). Using the measured contrast (2.8%) and width (22.25 MHz) of the rightmost peak in this spectrum, together with the photon count rate for this diamond particle ($\sim 1 \times 10^6$ per second), the estimated magnetic sensitivity of this diamond sensor is $19.9 \mu\text{T}/\sqrt{\text{Hz}}$ ^[23] at 9.1 GPa. This value means that a small magnetic field of $\sim 20 \mu\text{T}$ could be detected with this diamond magnetometer, within a data acquisition time of 1 s. Such a small field could be generated from a magnetic particle with diameters of hundreds of nanometers (a point dipole

model).

All quantum control of spins, including coherence measurement and dynamic magnetic sensing, are based on Rabi oscillations. To measure Rabi oscillations under high pressures, firstly a green laser pulse of $20 \mu\text{s}$ polarizes the ensemble spins to the $m_S = 0$ state, then resonant microwave pulses of varied duration are applied, to drive coherent oscillation of the NV spins. Finally, the spin state is read out by counting the photon number of the fluorescence signal under a second laser excitation, and an adjacent count is recorded to normalize the signal. Figures 2(c)–2(d) show typical Rabi oscillations of the ensemble NV spins under high pressures, the measured Rabi frequency of $\Omega = 40.8$ MHz at 32.8 GPa indicates the good efficiency of the microwave transmission line inside the DAC. The Rabi signal envelop decays exponentially, due to the large inhomogeneous broadening of the spin ensemble (~ 20 MHz for the measured NV centers, see Fig. 2(b)). Nevertheless, the coherent oscillations still last for more than $1 \mu\text{s}$, which enables lots of coherent measurements under high pressure.

The spin coherence and spin relaxation properties of the NV ensemble under high pressure are shown in Figs. 2(e) and 2(f). The π and half- π pulse parameters used are extracted from the Rabi oscillations (Fig. 2(c)). To determine the phase coherence time, the spin ensemble is prepared to a superposition state, $\frac{1}{\sqrt{2}}(|0\rangle + |1\rangle)$, and a π flip is applied to cancel static noise during the free evolution (Hahn echo sequence). An exponential decay fitting gives the phase coherence time of $T_2 = 2.5 \pm 0.2 \mu\text{s}$, which is dominated by the fast-flipping bath of surrounding P_1 centers. For spin relaxation measurement (T_1 process), the residual population of the $m_S = 0$ state is measured as a function of the evolution time, as shown in Fig. 2(f). The spin relaxation of the spin ensemble is $T_1 = 2.6 \pm 0.3$ ms. Both the spin coherence time and the spin relaxation time are similar to those measured under atmosphere pressure, indicating the robustness of the diamond quantum sensor.

We now turn to high-pressure magnetic sensing experiments. The magnetic sample is a small piece of $\text{Nd}_2\text{Fe}_{14}\text{B}$ polycrystal. $\text{Nd}_2\text{Fe}_{14}\text{B}$ is a type of material with a large magnetic moment, and is a permanent magnet widely used in various fields. It undergoes a ferromagnetic-paramagnetic Curie transition near 586 K.^[30] The Nd and Fe both contribute to the magnetic behavior: Nd is expected to have a magnetic moment of $3.3 \mu_B/\text{atom}$ while Fe atoms have been reported as having magnetic moments in the range of 2.1 – $2.9 \mu_B/\text{atom}$.^[31] Since this compound is an alloy, its magnetic behavior is very sensitive to the atomic distance, and a previous study has shown that pressure can drive a possible ferromagnetic-paramagnetic phase transition approximately at room temperature, near 10 GPa.^[32] Figure 3(a) shows a confocal image of

the DAC culet after loading the magnetic sample, in which the red dashed line circles the edge of the magnetic sample (obtained by comparing the confocal and bright-field images). Both the ruby and diamond particles emit fluorescence under green laser excitation, but the significant size difference makes them easy to distinguish from each other. The confocal image gives spatial resolution of $\sim 2\ \mu\text{m}$, which can be further improved by decreasing the distance between the sample and objective (using a high-NA objective).

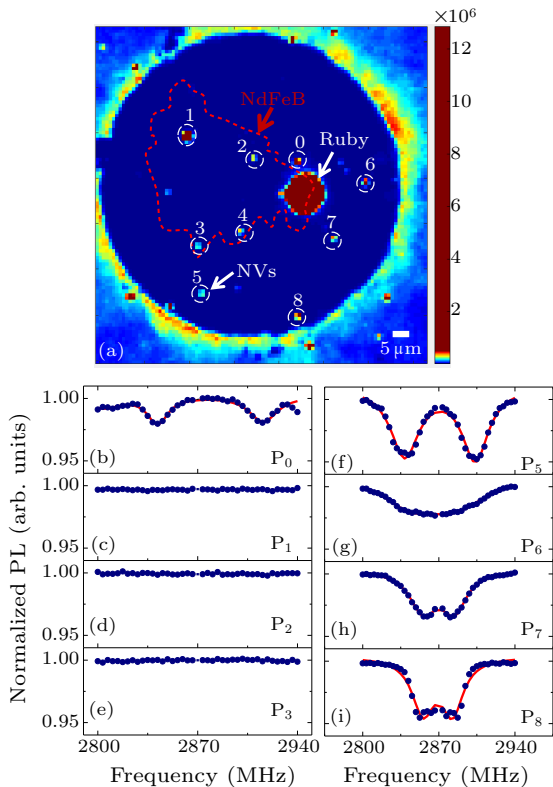


Fig. 3. Magnetic field distribution of the $\text{Nd}_2\text{Fe}_{14}\text{B}$ sample in the DAC. (a) Confocal image of the DAC culet after loading the $\text{Nd}_2\text{Fe}_{14}\text{B}$ sample, the ruby, and the diamond particles. The red dashed line circles the edge of the $\text{Nd}_2\text{Fe}_{14}\text{B}$ sample, the small bright spots inside the white open circles are μm -scale diamond particles with ensemble NV centers, and the big red circle is the ruby particle for pressure calibration. The spatial resolution of this image is $\sim 2\ \mu\text{m}$. (b)–(i) Zero-field ODMR spectra of ensemble NV centers in the μm -scale diamond particle. The ODMR contrast of particles at positions 1, 2 and 3 are quenched by the strong magnetic field, as they are right below the magnetic sample. For NV centers at other positions, the splitting and width of their ODMR spectra are also modified by the magnetic field of the $\text{Nd}_2\text{Fe}_{14}\text{B}$ sample.

To demonstrate the spatial-resolved quantum sensing of the stray magnetic field from the magnetic sample, we first measure the ODMR spectra of several diamond particles inside the DAC, with no external magnetic field. Typical zero-field ODMR spectra are presented in Figs. 3(b)–3(i). For NV centers right below the magnetic sample (positions 1–4 in Fig. 3(a)), the magnetic field is so strong that the ODMR contrast is almost quenched, consistent with the strong magnetic

character of $\text{Nd}_2\text{Fe}_{14}\text{B}$ at room temperature. For NV centers farther away from the magnetic sample (positions 5–8), small splitting and broadening features are observed, indicating the fast decay of the stray magnetic field from the measured sample. We then choose a diamond particle (position 0, at the edge of the magnetic sample) to track the sample magnetism in the following compression and decompression measurements, as the stray magnetic field at this position is large and still measurable.

The ODMR spectra of the compression process are summarized in Fig. 4(a). To avoid the extra splitting and broadening of ODMR spectra introduced by the non-hydrostatic pressure (see Fig. 1(c)), we employ a relatively large external magnetic field (145 Gauss) in the compression and decompression experiments. The orientation of the bias field is tuned to make the total magnetic field at position 0 along one of the N–V axes (at 1 GPa), and the NV centers of the other three orientations have the same resonant frequency under this magnetic field, as shown by the bottom line of Fig. 4(a). As the pressure increases, a smooth phase transition is clearly observed. The ODMR spectra show little change when the pressure is < 4 GPa, then a sharp shift of the resonant dips occurs in the range of 5–10 GPa, and then the spectra remain almost unchanged with further increasing pressure.

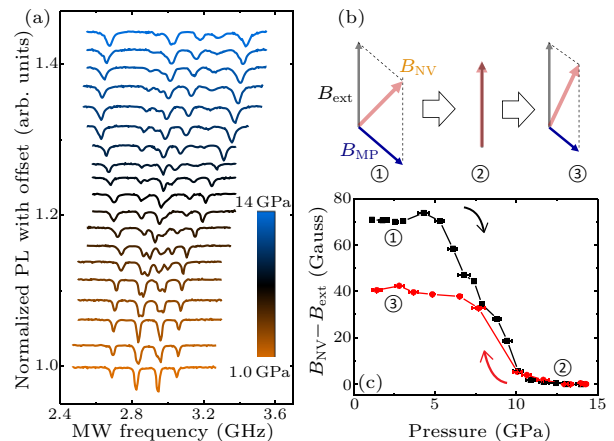


Fig. 4. Pressure-induced magnetic phase transition of the $\text{Nd}_2\text{Fe}_{14}\text{B}$ sample. (a) Continuous-wave ODMR spectra for ensemble NV centers inside the particle at position 0 (see Fig. 3 for its position) recorded during the compression process. The external magnetic field (145 Gauss) is tuned to make the total magnetic field at position 0 is along one of the N–V axes at $P = 1$ GPa. As the pressure increases, the magnetic field from the $\text{Nd}_2\text{Fe}_{14}\text{B}$ sample decreases, and the resonant frequencies of the ODMR spectra shift accordingly. (b) Schematic of the magnetic field vectors at different pressures: (1) low pressure before compression, (2) high pressure, (3) low pressure after decompression. (c) Magnetic field–pressure curves for the $\text{Nd}_2\text{Fe}_{14}\text{B}$ samples extracted from the ODMR spectra.

The magnetic field at position 0 is extracted from the measured ODMR spectra. First, the pressures are calibrated using the Raman signal from the ruby particle, and the zero-field splitting frequencies D of

the NV centers under pressure are obtained by referring to the measured D - P relations (Fig. 1(c) insert). Using the zero-field splitting value and the two outer resonant dips of the ODMR spectra, the temporal magnetic field strength is calculated, as summarized in Fig. 4(c). The B - P curve clearly shows the pressure-induced demagnetization of the $\text{Nd}_2\text{Fe}_{14}\text{B}$ sample. The decompression process is also measured, as summarized in the same figure, the magnetic field partially recovered as the pressure is released.

The significant $\text{Nd}_2\text{Fe}_{14}\text{B}$ magnetism changes under pressure accord with previous results.^[32] Magnetism suppression has been reported as being very common for $\text{Nd}_2\text{Fe}_{14}\text{B}$ compounds, and some Fe-based alloys.^[29] The long-range exchange coupling among Fe-Fe atoms is critical for Curie temperature determination, which shows a negative value to be consistent with the features of itinerant ferromagnetism.^[33] External pressure shortens the atomic distance among Fe atoms, weakening the spin polarization and exchange coupling, which thus drives the Curie temperature to lower temperatures. In our work, we find that the $\text{Nd}_2\text{Fe}_{14}\text{B}$ magnetic signal starts to weaken above 6 GPa, and enters another magnetic state above 10 GPa, which shows a weak pressure dependence (Fig. 4(b)). Based on these results, we would like to claim that $\text{Nd}_2\text{Fe}_{14}\text{B}$ undergoes a ferromagnetic-paramagnetic phase transition near 10 GPa at room temperature. In other words, the pressure has pushed the Curie temperature from its original 586 K to room temperature at 10 GPa.

During the pressure releasing process, we find that the B - P trend is well consistent with that of the compression process, with the only difference that the stray magnetic field is slightly smaller during the pressure releasing process. This change is mainly due to the different magnetization process of the $\text{Nd}_2\text{Fe}_{14}\text{B}$ sample during compression and decompression. The original sample is from a commercial product, which has been magnetized by a large magnetic field and carries a huge remnant moment. However, the sample is demagnetized and entered a paramagnetic state above 10 GPa and is then re-magnetized by a small external magnetic field of only 145 Gauss, which is much smaller than the coercive field for $\text{Nd}_2\text{Fe}_{14}\text{B}$. Hence, the sample only carries a weak remnant moment during the decompression process and shows a weaker magnetic signal in comparison with its original state.

In the above proof-of-principle experiment, the sample is a strong magnetic material. For samples with weak magnetic signal (such as canted or collinear antiferromagnetic materials), their static magnetic field could be enhanced with an external magnetic field and then detected with the same method (ODMR spectrum). We would like to emphasize that the NV-based quantum sensor is also a good magnetic noise spectroscopy, which can be used to study dynamic

magnetic properties of a sample, even there is no macro magnetism. At the surface of a sample, there are characteristic magnetic fluctuations determined by the magnetic phases of the material (even in a paramagnetic state). Such magnetic noise will alter the spin coherence of NV centers (close to the sample) thus can be detected. Typical dynamic magnetic sensing techniques include NV spin relaxation, spin coherence, and correlation measurement of the NV spin states.^[14]

To study the superconductivity of hydride compounds, quantum sensors with working pressures >100 GPa are needed.^[7-9] The current experiment has demonstrated coherent quantum control of diamond NV center spins up to 32.8 GPa. As the pressure increases, the zero-phonon line of diamond NV center shifts to the short-wave side.^[12] Doherty *et al.* demonstrated that ODMR spectra could be obtained up to 60 GPa, and higher working pressures could be expected as shorter wavelength excitation lasers (<532 nm) are used. Another interesting upgrade of the high-pressure ODMR technique is the integration of laser heating to DAC. NV center is a good thermometer in the temperature range from mK to 1000 K,^[16] and laser heating is well developed for DAC-based experiment. By combining these two techniques, high temperature and high pressure (HTHP) experiments with *in situ* sensitive sensors could be achieved. Such facilities would enable direct measurement of the P - T phase diagram in a large parameter range, with reasonably good sensitivity to physical parameters, including magnetic field, electric field, pressure, and temperature. HTHP experiments are of crucial importance in the fields of earth science and geophysics, since the interior of earth is an HTHP environment.

In summary, we have demonstrated fast coherent manipulation of ensemble NV spins, up to 32.8 GPa, and the measured spin coherence and spin relaxation time have little difference as compared to those measured under ambient conditions. We have used *in situ* and sensitive quantum sensors to study the pressure-induced magnetic phase transition of $\text{Nd}_2\text{Fe}_{14}\text{B}$. To improve the spatial resolution and reusability of the DAC chamber, shallow NV centers on the diamond culet could be employed. To improve microwave transmission efficiency, coplanar waveguides could be deposited on the DAC culet, which is compatible with much higher pressures.

References

- [1] Mao H K, Chen X J, Ding Y, Li B and Wang L 2018 *Rev. Mod. Phys.* **90** 015007
- [2] Kuhs W F, Finney J L, Vettier C and Bliss D V 1984 *J. Chem. Phys.* **81** 3612
- [3] Santoro M, Gregoryanz E, Mao H and Hemley R J 2004 *Phys. Rev. Lett.* **93** 265701
- [4] Dalladay-Simpson P, Howie R T and Gregoryanz E 2016 *Nature* **529** 63

- [5] Hamlin J J 2015 *Physica C* **514** 59
- [6] Ashcroft N W 1968 *Phys. Rev. Lett.* **21** 1748
- [7] Ashcroft N W 2004 *Phys. Rev. Lett.* **92** 187002
- [8] Somayazulu M, Ahart M, Mishra A K, Geballe Z M, Bal-dini M, Meng Y, Struzhkin V V and Hemley R J 2019 *Phys. Rev. Lett.* **122** 027001
- [9] Drozdov A P, Kong P P, Minkov V S, Besedin S P, Kuzovnikov M A, Mozaffari S, Balicas L, Balakirev F F, Graf D E, Prakapenka V B, Greenberg E, Knyazev D A, Tkacz M and Eremets M I 2019 *Nature* **569** 528
- [10] Jayaraman A 1983 *Rev. Mod. Phys.* **55** 65
- [11] Alireza P L and Julian S R 2003 *Rev. Sci. Instrum.* **74** 4728
- [12] Doherty M W, Struzhkin V V, Simpson D A, McGuinness L P, Meng Y, Stacey A, Karle T J, Hemley R J, Manson N B, Hollenberg Lloyd C and Prawer S 2014 *Phys. Rev. Lett.* **112** 047601
- [13] Acosta V M, Bouchard L S, Budker D, Folman R, Lenz T, Maletinsky P, Rohner D, Schluskel Y and Thiel L 2019 *J. Supercond. Novel Magn.* **32** 85
- [14] Degen C L, Reinhard F and Cappellaro P 2017 *Rev. Mod. Phys.* **89** 035002
- [15] Casola F, Van Der Sar T and Yacoby A 2018 *Nat. Rev. Mater.* **3** 17088
- [16] Liu G Q, Feng X, Wang N, Li Q and Liu R B 2019 *Nat. Commun.* **10** 1344
- [17] Aslam N, Pfender M, Stöhr R, Neumann P, Scheffler M, Sumiya H, Abe H, Onoda S, Ohshima T, Isoya J and Wrachtrup J 2015 *Rev. Sci. Instrum.* **86** 064704
- [18] Hsieh S, Bhattacharyya P, Zu C, Mittiga T, Smart T J, Machado F, Kobrin B, Höhn T O, Rui N Z, Kam-rani M, Chatterjee S, Choi S, Zaletel M, Struzhkin V V, Moore J E, Levitas V I, Jeanloz R and Yao N Y 2018 [arXiv:1812.08796v1](https://arxiv.org/abs/1812.08796v1)[cond-mat.mes-hall]
- [19] Lesik M, Plisson T, Toraille L, Renaud J, Occelli F, Schmidt M, Salord O, Delobbe A, Debuisschert T, Rondin L, Loubeyre P and Roch J F 2018 [arXiv:1812.09894v1](https://arxiv.org/abs/1812.09894v1)[cond-mat.mes-hall]
- [20] Yip K Y, Ho K O, Yu K Y, Chen Y, Zhang W, Kasahara S, Mizukami Y, Shibauchi T, Matsuda Y, Goh S K and Yang S 2018 [arXiv:1812.10116v1](https://arxiv.org/abs/1812.10116v1)[cond-mat.mes-hall]
- [21] Acosta V M, Bauch E, Ledbetter M P, Waxman A, Bouchard L S and Budker D 2010 *Phys. Rev. Lett.* **104** 070801
- [22] Schirhagl R, Chang K, Loretz M and Degen C L 2014 *Annu. Rev. Phys. Chem.* **65** 83
- [23] Rondin L, Tetienne J P, Hingant T, Roch J F, Maletinsky P and Jacques V 2014 *Rep. Prog. Phys.* **77** 056503
- [24] Zhao N, Hu J L, Ho S W, Wan J T K and Liu R B 2011 *Nat. Nanotechnol.* **6** 242
- [25] Arai K, Belthangady C, Zhang H, Bar-Gill N, DeVience S J, Cappellaro P, Yacoby A and Walsworth R L 2015 *Nat. Nanotechnol.* **10** 859
- [26] Boss J M, Cujia K S, Zopes J and Degen C L 2017 *Science* **356** 837
- [27] Schmitt S, Gefen T, Stürner F M, Unden T, Wolff G, Müller C, Scheuer J, Naydenov B, Markham M, Pezzagna S, Meijer J, Schwarz I, Plenio M, Retzker A, McGuinness L P and Jelezko F 2017 *Science* **356** 832
- [28] Pfender M, Wang P, Sumiya H, Onoda S, Yang W, Dasari D B R, Neumann P, Pan X Y, Isoya J, Liu R B and Wrachtrup J 2019 *Nat. Commun.* **10** 594
- [29] Mao H K and Bell P M 1976 *Science* **191** 851
- [30] Hirose S, Matsuura Y, Yamamoto H, Fujimura S, Sagawa M and Yamauchi H 1986 *J. Appl. Phys.* **59** 873
- [31] Nordström L, Johansson B and Brooks M S S 1991 *J. Appl. Phys.* **69** 5708
- [32] Kamarád J, Arnold Z and Schneider J 1987 *J. Magn. Magn. Mater.* **67** 29
- [33] Toga Y, Matsumoto M, Miyashita S, Akai H, Doi S, Miyake T and Sakuma A 2016 *Phys. Rev. B* **94** 174433